

# Waveguide source of correlated photon-pairs for chip-scale quantum information processing

Jun Chen,<sup>a,b\*</sup> Aaron J. Pearlman,<sup>a</sup> Alexander Ling,<sup>a,b</sup> Jingyun Fan,<sup>a,b†</sup> and Alan Migdall<sup>a,b</sup>

<sup>a</sup> Optical Technology Division, National Institute of Standards and Technology  
100 Bureau Drive, Gaithersburg, MD 20899-8441, U.S.A.

<sup>b</sup> Joint Quantum Institute, University of Maryland, College Park, MD 20742, U.S.A.

## ABSTRACT

We present a systematic study of a correlated photon-pair source based on a periodically-poled KTiOPO<sub>4</sub> (PPKTP) waveguide. The waveguide was fabricated on a KTiOPO<sub>4</sub> crystal supporting type-II parametric down-conversion. In addition, periodic poling was applied along the waveguide to quasi-phase-match the type-0 down-conversion process. The design pump wavelength is 532 nm, and the wavelengths of the down-converted, correlated photons are around 900 nm and 1300 nm. We examine the two-photon correlation spectra and single-photon spectra at a variety of temperature and power settings for both type-0 and type II down-conversion processes. Our study shows that the waveguide source has a number of advantages compared to its bulk-crystal counterpart, including higher spectral brightness, narrower emission bandwidth and single spatial-mode output. With greatly simplified engineering, this compact, highly efficient, low photon-loss, and cost-effective waveguide source of correlated photon pairs is promising for future chip-scale quantum information processing applications.

**Keywords:** spontaneous parametric down conversion, correlated photons, waveguide, joint spectrum

## 1. INTRODUCTION

Photon pairs have played an essential role in many modern quantum-optical applications such as entanglement generation,<sup>1–4</sup> heralded single-photon sources,<sup>5,6</sup> and linear optical quantum computing.<sup>7,8</sup> Recently, spontaneous parametric down-conversion (SPDC) in periodically-poled nonlinear waveguides has been shown to be an efficient way to generate such correlated photon pairs.<sup>9–13</sup> SPDC is a second-order [ $\chi^{(2)}$ ] nonlinear process wherein a pump photon is absorbed and a pair of energy- and momentum-conserving daughter photons (referred to as signal and idler) are generated, satisfying  $\omega_p = \omega_s + \omega_i$  and  $\vec{k}_p = \vec{k}_s + \vec{k}_i$ , where  $\omega_{p,s,i}$  and  $\vec{k}_{p,s,i}$  are the photon frequencies and wave-vectors, and the subscripts p, s, and i stand for pump, signal, and idler, respectively. Compared with its bulk-crystal counterpart which inherently generates photon pairs into multiple spatial modes,<sup>1</sup> SPDC in waveguides outputs photon pairs collinearly, with a predominant component in the fundamental single spatial mode of the waveguide.<sup>9,12</sup> This facilitates efficient coupling of these photons into single-mode optical fibers, and offers the potential to make chip-scale devices for quantum-information-processing applications.

Fully realizing the potential of such a chip-scale quantum device requires understanding of its various operating modes, such as the temperature and pump-polarization dependencies of the photon-pair production rate. More importantly, for wavelength-division-multiplexing applications that use many wavelength pairs simultaneously,<sup>14,15</sup> one needs to have precise knowledge of the coincidence spectra (also called joint spectra),<sup>16–19</sup> and be able to separate true signal (photon pairs) from random noise (single-photon fluorescence<sup>6,12</sup>). This critical information is missing from the current literature. Here we systematically study a waveguided photon-pair source. Both photon-pair and single-photon emission spectra, as well as their dependence on input-pump polarization and waveguide temperature, are obtained for both type-0 and type-II phase-matching SPDC processes in a single PPKTP waveguide.

---

Further author information: (Send correspondence to junchen@nist.gov or jfan@nist.gov)

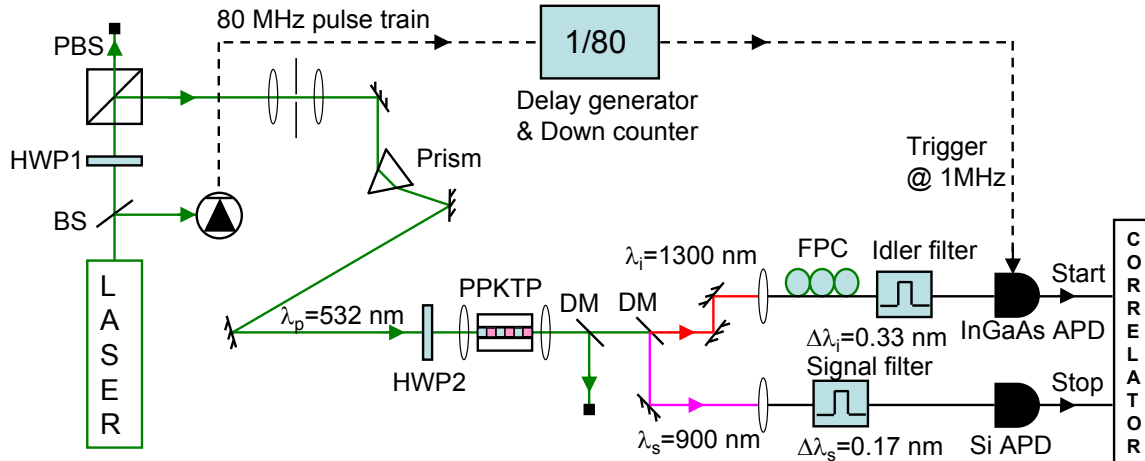


Figure 1: Diagram of the experimental setup. A PPKTP waveguide is pumped with a pulsed laser, and the down-converted photons are spectrally analyzed using tunable filters and coincidence detection with single-photon detectors. BS, beam splitter; PBS, polarizing beam splitter; DM, dichroic mirror; HWP, half-wave plate; FPC, fiber polarization controller; APD, avalanche photodiode.

## 2. EXPERIMENTAL SETUP

Our experimental setup is shown schematically in Fig. 1. The pump beam, derived from an 80-MHz pulsed laser with  $\lambda_p = 532.2$  nm and a 5-ps pulse width, is sent through a spatial filter and a prism to ensure that the PPKTP waveguide is pumped with a single spatial-mode and spectrally clean beam (i.e., the pump beam does not contain any frequency components at either the signal or the idler frequencies). The waveguide is 1.5-cm long with a  $4 \times 4 \mu\text{m}^2$  cross section. It was fabricated on a flux-grown KTP crystal phase-matched for type-II SPDC ( $H_p \rightarrow V_s + H_i$ ,  $H$ : horizontal polarization,  $V$ : vertical polarization), and then periodically poled with a nominal grating period of  $\Lambda = 8.29 \mu\text{m}$  to additionally support type-0 ( $V_p \rightarrow V_s + V_i$ ) quasi-phase matching (QPM). QPM is enabled by periodically poling the nonlinear crystal so that the interaction length of the pump inside the crystal can be extended and a desired phase-matched set of wavelengths can be engineered, satisfying  $k_p = k_s + k_i + 2\pi m/\Lambda + k_{\text{wg}}$ ,<sup>12,20</sup> where  $m$ , an integer, is the  $m$ th order harmonic of the grating, and  $k_{\text{wg}}$  is the waveguide contribution to phase matching.<sup>12</sup> As a result, the waveguide can support both type-0 and type-II SPDC processes, with its emission field predominantly in a single spatial mode. Note that type-0 SPDC is only possible with the technique of QPM, whereas type-II SPDC is enabled by the unpoled KTP crystal itself. The existence of two types of SPDC is not directly related to our goal of providing precise characterization of waveguide-based coincidence spectra, but can be seen as an example of the waveguide's versatile ability to produce different kinds of two-photon states just by tuning the pump polarization. Measured values<sup>21</sup> of nonlinear - optical coefficients show that at the wavelength of  $1.064 \mu\text{m}$ ,  $d_{33} = 13.7$  pm/V (responsible for type-0 SPDC) and  $d_{24} = 7.6$  pm/V (responsible for type-II SPDC). The QPM-induced effective nonlinear-optical coefficient for type-0 SPDC is  $d_{\text{eff}} = \frac{2}{\pi} d_{33} \approx 8.7$  pm/V  $> d_{24}$ . This suggests that type-0 SPDC could be made potentially more effective than type-II SPDC, but as will be shown in our experimental results, the reverse is true for this particular waveguide at its phase-matched wavelengths.

At the waveguide input, a half-wave plate (HWP2 in Fig. 1) controls the pump polarization to switch between the two types of SPDC. The waveguide's temperature is controlled using a thermo-electric cooler with 0.01 °C stability. We use an aspheric lens [numerical aperture (NA) = 0.2] to couple pump light into the waveguide (NA  $\approx$  0.2), and a 10X microscope to couple out light of all wavelengths. The coupling efficiency of the pump into the waveguide is  $\approx$  30%. The daughter photons are separated from the pump beam and from each other by using two dichroic mirrors. Since the signal ( $\lambda_s \approx 900$  nm) and idler ( $\lambda_i \approx 1300$  nm) photons are quite different in wavelength, their spatial modes evolve differently when they emerge from the waveguide. We optimize the coupling of idler photons into a single-mode fiber by adjusting the output 10X microscope to nearly collimate its output. With the idler mode now optimized, the spatial mode of the signal photons is observed (using a

CCD camera) to be slightly converging, which we correct using a concave lens ( $f = -200$  mm, not shown in Fig. 1) before coupling into a separate single-mode fiber. The non-degeneracy of the signal and idler wavelengths made their separation from each other and the bright pump light easy to accomplish; we find that in practice two dichroic mirrors (DM in Fig. 1) are enough to provide the necessary pump rejection ( $> 100$  dB) to allow clean detection of the signal and idler photons. This particular set of wavelengths would be useful, for example, in a hybrid quantum communication system, wherein the idler photon ( $\approx 1300$  nm, a telecom wavelength) of a correlated pair propagates through a low-loss telecom fiber, and its sibling — the signal photon ( $\approx 900$  nm) — can be sent through free space with relatively low loss. Finally, both photons can be detected using high quantum efficiency single-photon detectors available with current technology.<sup>22–24</sup>

The filter system for the signal photons is a homemade double-grating filter with both a tunable central wavelength and an adjustable bandwidth, while for the idler photons we use a commercial fixed-bandwidth tunable filter. Both filters are computer controlled for automatic spectral scanning. The signal filter bandwidth is set to  $\Delta\lambda_s = 0.17$  nm to match the fixed bandwidth of the idler filter ( $\Delta\lambda_i = 0.33$  nm), so that they contain the same energy contents. After filtering, idler photons are detected with an InGaAs avalanche photodiode in gated Geiger mode, with a 1 MHz gate frequency and a gate width of 1.28 ns. The gating signal is obtained by using a beam splitter (BS in Fig. 1) to pick off part of the laser output, which is detected with an analog photodiode. The 80 MHz detection output is then sent through a down-counter/delay generator and converted to a 1 MHz pulse train with suitable delay. A fiber polarization controller (FPC in Fig. 1) is placed in front of the idler filter to maximize its transmission which is polarization dependent. Signal photons are detected with a silicon avalanche single-photon detector. Coincidences are recorded through start and stop inputs, with the detection pulses from the idler (signal) acting as the start (stop).

### 3. EXPERIMENTAL RESULTS

#### 3.1 Temperature dependence of single-photon spectra

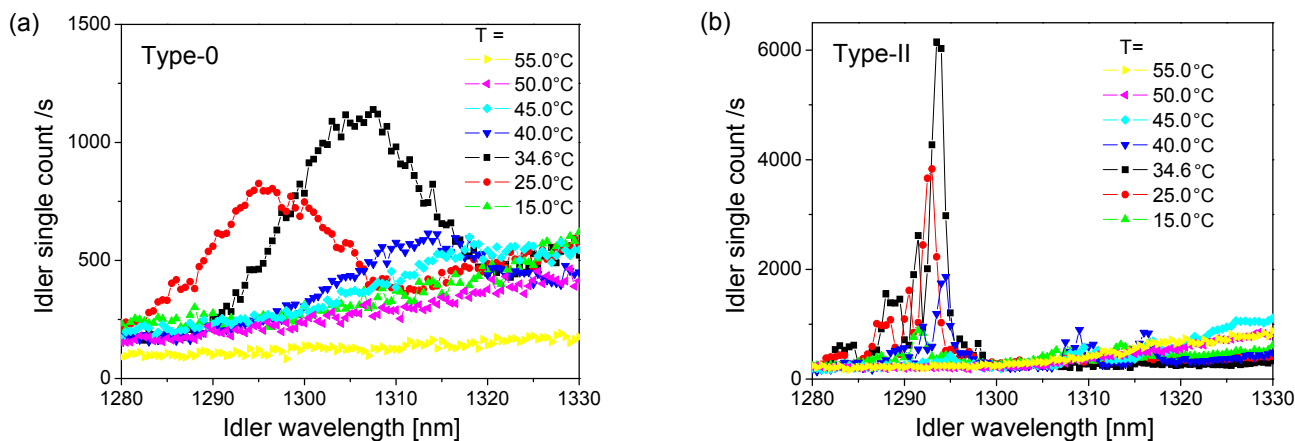


Figure 2: Temperature dependence of idler single-count spectrum for (a) type-0 SPDC, and (b) type-II SPDC.

The temperature dependencies of single-count idler spectra for both types of SPDC are shown in Fig. 2. We scan the computer-controlled idler-channel tunable filter for each waveguide temperature value (at a step size of 0.5 nm) and record the idler single counts. The average pump power exiting the waveguide is kept at 0.5 mW for both  $H$  and  $V$  pump polarizations. Note that these counts are taken without any measurement on the signal channel (i.e., they are not heralded counts). For both types of SPDC, we observe a dramatic dependence of single-photon production rate on temperature. While we cannot ascertain that all of the collected photons are produced by SPDC (in fact, a portion of them are produced by single-photon fluorescence due to defects in the waveguide<sup>6,12</sup>), we conjecture that the peaks in the single-photon spectra are much more likely to be caused by the SPDC photons rather than fluorescence, and they also correspond to peaks in the production of SPDC photon pairs. This conjecture is confirmed by measurements of the coincidence spectra in section 3.3. On the

other hand, at temperatures that do not allow efficient quasi-phase matching (e.g.,  $T = 55.0^\circ\text{C}$ ), almost all of the collected photons are produced by single-photon fluorescence, since no peak structure in the single-count spectrum is observable. We note in passing that the side peaks observed in Fig. 2(b) are possibly due to SPDC into higher-order spatial modes of the waveguide.<sup>25</sup> The main peak, corresponding to the fundamental mode, is the dominant component of the output spectra, and can be well isolated from higher-order modes by using spectral and/or spatial filtering.

Comparing Fig. 2(a) and (b), we can see that: (i) both types of SPDC have an optimal operating temperature, which is nearly the same ( $T_{\text{opt}} = 34.6^\circ\text{C}$ ); (ii) type-0 SPDC has a much wider phase-matching bandwidth [full width at half maximum (FWHM)  $\approx 12\text{ nm}$  for idler] than type-II SPDC (FWHM  $\approx 1.4\text{ nm}$  for idler); (iii) type-II SPDC is spectrally brighter (5X) than type-0 SPDC at their peak values, but (iv) in terms of the overall brightness (i.e., unfiltered output), we find that type-II is only slightly brighter ( $\sim 7\%$ ) than type-0 at the optimal temperature  $T_{\text{opt}}$ . The same characteristics are also seen in the signal single-count spectra (not shown). We acknowledge that it is an unexpected coincidence that both type-0 and type-II SPDC are optimally phase matched at nearly the same temperature. While it is possible that this is simply a coincidence, it is more likely that there is some physical reason, which we have not yet identified at this point. As to the differences in terms of bandwidths and brightnesses between Fig. 2(a) and (b), a combination of two factors is responsible. First, since the PPKTP waveguide is birefringent, a horizontally-polarized pump travels at a different group velocity than a vertically-polarized pump, and therefore must satisfy a different phase-matching condition for efficient down-conversion, which gives rise to the different phase matching bandwidths for the two types of SPDC. Second, the two types of SPDC processes rely on different second-order nonlinear susceptibility tensor components:  $\chi_{zzz}^{(2)}$  (or  $d_{\text{eff}} = \frac{2}{\pi}d_{33}$ ) for type-0 and  $\chi_{zyy}^{(2)}$  (or  $d_{24}$ ) for type-II. However, simply comparing the magnitudes of the nonlinear-optic coefficients would lead to the conclusion that type-0 is more efficient than type-II (since  $d_{\text{eff}} > d_{24}$ ), which is the opposite of what has been observed. We will compare the two SPDC phase-matching processes in more detail in section 3.5, and provide a possible reason for this.

### 3.2 Coincidence-to-accidental ratio

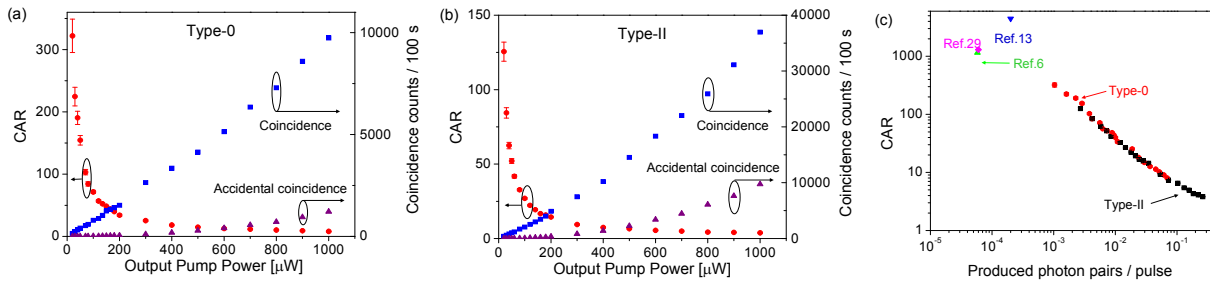


Figure 3: Pump power dependencies of CAR (left axis) and coincidences and accidental coincidences per 100 s (right axis) for (a) type-0 SPDC with  $\lambda_s = 899.18\text{ nm}$  and  $\lambda_i = 1304.00\text{ nm}$  and (b) type-II SPDC with  $\lambda_s = 904.00\text{ nm}$  and  $\lambda_i = 1294.00\text{ nm}$ . (c) Log-log plot of CAR vs. produced photon pairs per pulse. Three additional data points from external references are included for comparison. Detector dark-count contributions have been subtracted.

To collect the peak phase-matched SPDC photon pairs at the optimal temperature  $T_{\text{opt}}$ , we set the tunable filters in both channels. For type-0, we use the wavelength pair  $\{\lambda_s = 899.18\text{ nm}, \lambda_i = 1304.00\text{ nm}\}$ ; for type-II:  $\{\lambda_s = 904.00\text{ nm}, \lambda_i = 1294.00\text{ nm}\}$ . For each wavelength pair, we varied the pump power (by rotating HWP1 in Fig. 1) and recorded coincidences and accidental coincidences at each pump power level. The coincidence-to-accidental ratio (CAR), a commonly used two-photon source purity measure,<sup>26–29</sup> is plotted as a function of the output pump power in Fig. 3. The CAR values for our source for both types of SPDC are comparable with other sources at similar pair production rates.<sup>6,13,30</sup> The CAR also shows a trend common to the other photon sources: it monotonically decreases with increasing pump power. This is understood because the coincidence counts per pulse  $C$  is roughly proportional to the pump power  $P$  (i.e.,  $C \propto P$ ), whereas accidental coincidence counts per pulse  $A$  scales as  $P^2$  (i.e.,  $A \propto P^2$ ), so  $\text{CAR} \equiv C/A \propto 1/P$ . Note that with a wider filter bandwidth, the CAR will generally decrease because more uncorrelated photons are collected in the process.<sup>31</sup>

We see that type-II SPDC has a lower CAR than type-0 SPDC at the same pump power; however, this is because type-II SPDC produces more coincidences than type-0 SPDC at the same pump power. In other words, type-II SPDC is more efficient than its type-0 counterpart in this waveguide, so it requires a lower pump power to achieve the same CAR. Indeed, if we plot CAR against pair production efficiency (i.e., produced photon pairs per pulse) as shown in Fig. 3(c), we can see that the two SPDC processes have about the same CAR at the same level of pair production efficiency. A high CAR, which suggests a high-purity photon-pair source, can be achieved for both types of SPDC when the waveguide is pumped with relatively low peak pump power, which incurs low pair production per pulse. Of course, the photon pair production rate (i.e., pairs/s) can still be made quite high if one uses a high-repetition-rate pump laser (see for instance Ref. [13]).

To compare our source with other photon pair sources, we include three additional data points in Fig. 3(c) from Ref. [6] (type-II SPDC in a PPKTP waveguide), Ref. [13] (quasi-phase matched SPDC in a PPLN waveguide), and Ref. [30] (four-wave mixing in a liquid-helium-cooled dispersion-shifted fiber). Fig. 3(c) clearly shows the tradeoff between CAR and the pairs per pulse production rate. By extrapolating our CAR-vs.-production-rate data, we can see that our source outperforms those in Refs. [6] and [30] with the possible exception of the source in Ref. [13]. This could be due to a number of reasons, including less emission of noise photons, lower propagation loss, and higher photon-pair production efficiency in the PPLN waveguide.

### 3.3 Coincidence spectra

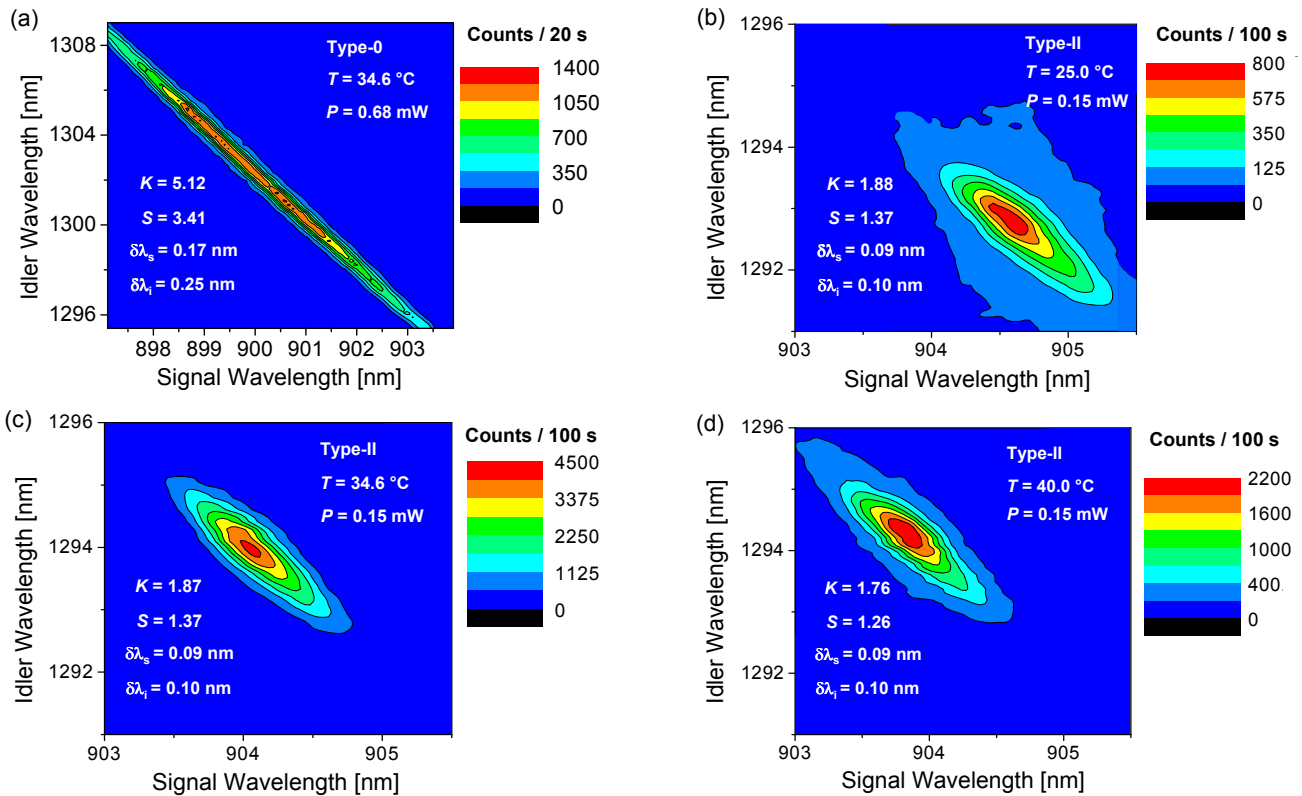


Figure 4: Coincidence spectra for (a) type-0 SPDC at  $T_{\text{opt}} = 34.6\text{ }^{\circ}\text{C}$ , type-II SPDC at (b)  $T = 25.0\text{ }^{\circ}\text{C}$ , (c)  $T_{\text{opt}} = 34.6\text{ }^{\circ}\text{C}$ , and (d)  $T = 40.0\text{ }^{\circ}\text{C}$ . Note that while the range and scale of (a) are different from (b), (c), and (d), the aspect ratio is constant at 2:1 for all; and although the power  $P$  and counting time  $t$  of (a) are different from (b), (c), and (d), their product  $Pt$  is roughly the same for all, so that the results can be directly compared. The Schmidt number  $K$  and entropy of entanglement  $S$  are also indicated on each figure.

The spectra presented in section 3.1 are useful for identifying the optimum operating temperatures for the waveguide. However, as we have pointed out, single-photon spectra do not distinguish between photons that come

from single-photon fluorescence and those generated in a SPDC process. A standard technique to discriminate against single-photon fluorescence is to measure coincidences during a spectral scan.<sup>32</sup> Single-photon fluorescence will not generate coincidence counts except by accident (such events are known as accidental coincidences, and can be generated by, e.g., a coincidence between a detector dark count and a registered single-photon fluorescence).

Furthermore, it is known that Type-II SPDC pumped by a pulsed (and hence broadband) laser results in spectrally distinguishing properties for the down-converted photons.<sup>16</sup> When correlated photon pairs from such a pulsed source are used to generate polarization-entangled photon pairs, this distinguishing information will reduce the obtainable entanglement. Such spectral properties show up readily in a coincidence-based spectral scan, which we call the coincidence spectrum (or joint spectrum, as they reveal the joint spectral properties of the correlated photon pair). Although several groups have studied the coincidence spectra of pulsed Type-II sources pumped by ultrafast lasers (pulse duration  $\approx 10 - 200$  fs),<sup>17,18</sup> no such spectra exist for sources based on waveguides that are pumped with slower pulses ( $\approx 2 - 10$  ps), the regime where we operate. To understand whether the spectral features present in ultrafast sources also exist in our system, we have mapped out the coincidence spectra for both type-0 and type-II SPDC processes.

To measure a coincidence spectrum of each type of SPDC, we use two narrow-band computer-controlled tunable filters, one in each collection arm.<sup>33</sup> Stepping through the signal and idler wavelength ranges, we record coincidence counts for each  $\{\lambda_s, \lambda_i\}$  pair with  $\{\Delta\lambda_s, \Delta\lambda_i\}$  resolution at a discrete step size of  $\{\delta\lambda_s, \delta\lambda_i\}$ . The results are color-coded as 2-dimensional coincidence spectra shown in Fig. 4. The wavelength resolutions are kept the same for all measurements ( $\Delta\lambda_s = 0.17$  nm,  $\Delta\lambda_i = 0.33$  nm), and the step sizes used in obtaining each coincidence spectrum are indicated on the figures. Note that the resolutions in this experiment are limited not by our homemade signal grating filter, but by the fixed passband of the commercial idler filter.

We also include two important quantities on each coincidence spectrum, namely, the Schmidt number  $K$  (also known as the cooperativity parameter) and the entropy of entanglement  $S$ .<sup>34,35</sup> They quantify how much spectral entanglement (or nonseparability) exists in a given two-photon state  $\Psi(\lambda_s, \lambda_i)$ , and can be conveniently calculated from its coincidence spectrum through Schmidt decomposition.<sup>36</sup> In terms of the normalized Schmidt eigenvalues  $\lambda_n$  (i.e.,  $\sum_n \lambda_n = 1$ ), the Schmidt number is defined as  $K = 1/(\sum_n \lambda_n^2)$  and the entropy of entanglement is given by  $S = -\sum_n \lambda_n \log_2(\lambda_n)$ . Both of these increase monotonically with the amount of spectral entanglement present in  $\Psi(\lambda_s, \lambda_i)$ . They achieve their minimum values ( $K_{\min} = 1$  and  $S_{\min} = 0$ ) for a factorable two-photon state [i.e.,  $\Psi(\lambda_s, \lambda_i) = \psi(\lambda_s)\phi(\lambda_i)$ , possessing zero spectral entanglement], which is an important resource for quantum information applications such as heralded pure single-photon states<sup>35</sup> and multi-element Hong-Ou-Mandel interference.<sup>37</sup> The Schmidt number is estimated to be 5.12 for the type-0 two-photon state shown in Fig. 4(a), indicating a high degree of spectral entanglement. In comparison, the Schmidt numbers are much lower ( $K \approx 1.8$ ) for the type-II two-photon states shown in Fig. 4(b), (c) and (d). This means that the type-II two-photon state is less spectrally entangled than its type-0 counterpart in this waveguide, and thus more closely approaches a factorable state. This suggests that a factorable two-photon state output may be possible through waveguided SPDC. We have also numerically simulated the two-photon joint spectra using the phase-matching equations in section 3.5, and have found very good agreement between the measured and the simulated coincidence spectra (not shown).

Comparing Fig. 4(a) and (c), we can see that type-0 SPDC has a wider phase-matching bandwidth, but is spectrally dimmer than type-II SPDC, which is consistent with the single-count data shown in Fig. 2. Comparisons among Fig. 4(b), (c), and (d) reveal that the coincidence spectrum maintains its characteristic shape at different temperatures, although with some changes in the peak count rate and the peak wavelengths. They also show that the optimal temperature for type-II single-photon [Fig. 2(b)] and pair production is the same. We have also taken coincidence spectra for type-0 SPDC at different temperatures (not shown), which point to the same conclusion. This proves our initial conjecture posed in section 3.1, namely, the two optimal temperatures coincide. It is noteworthy that the shape of the coincidence spectra is very similar to the spectra of CW-based sources,<sup>17,19</sup> and unlike the irregular shaped spectra reported with ultrafast sources.<sup>18</sup> The similarity between our source and the CW sources can be understood since our pump bandwidth is relatively narrow ( $\approx 0.2$  nm) and can be effectively treated as quasi-CW. The difference between our source and ultrafast sources can be mainly attributed to the different pump bandwidths and the different phase-matching curves for the materials involved. Nevertheless, this means that spectral distinguishability is not an issue when considering if a waveguide pumped

with picosecond lasers can be used as a source for polarization-entangled photon pairs. Although both types of SPDC contain some degree of spectral entanglement (as evidence by the non-vanishing  $S$  in both cases), tight spectral filtering can be applied to reduce the amount of spectral entanglement to allow efficient quantum information processing applications such as polarization entanglement swapping, at the cost of reduced coincidence count rates.

### 3.4 Photon pair and single-photon fluorescence

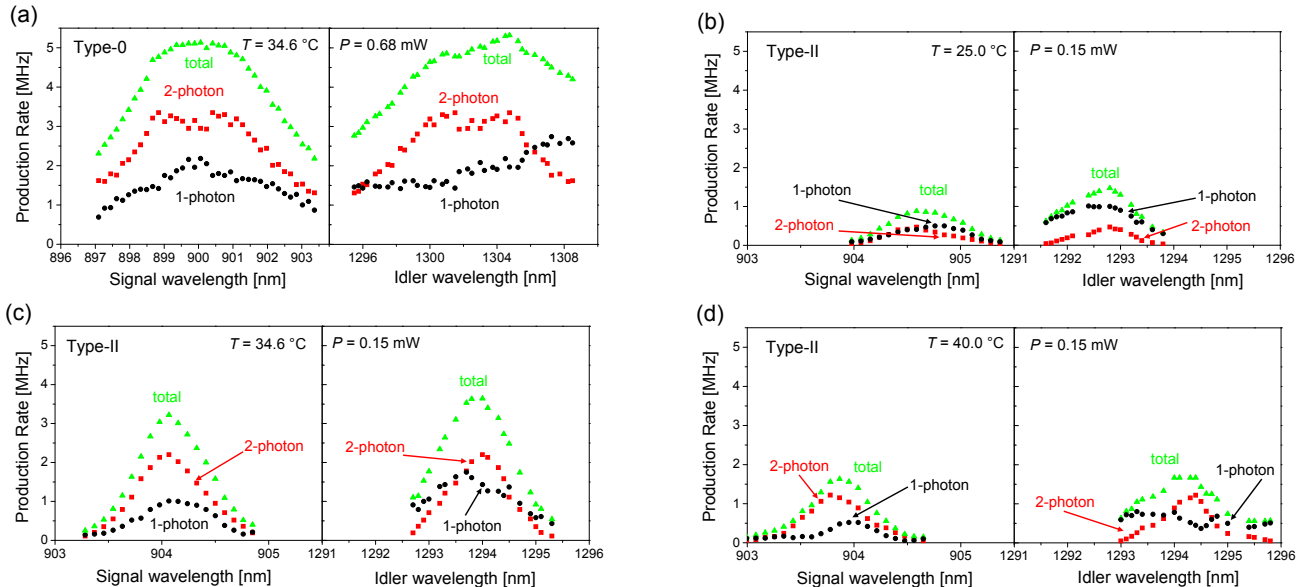


Figure 5: Single-count spectra for (a) type-0 SPDC at  $T_{\text{opt}} = 34.6^\circ\text{C}$ , type-II SPDC at (b)  $T = 25.0^\circ\text{C}$ , (c)  $T_{\text{opt}} = 34.6^\circ\text{C}$ , and (d)  $T = 40.0^\circ\text{C}$ . Note that the production rate is plotted instead of the detected rate. Photon-pair (2-photon) and single-photon background (1-photon) contributions are distinguished using experimentally determined total collection efficiencies.

Table 1: Measured values of transmission efficiencies for optical path components and the single-photon detection efficiencies. The uncertainties are one standard deviation.

Component	Channel efficiencies (%)	
	Signal	Idler
Waveguide out-coupling	$91 \pm 1$	$80 \pm 1$
Free-space optics	$82 \pm 1$	$76 \pm 1$
Fiber coupling	$25 \pm 2$	$45 \pm 2$
Filter transmission	$50 \pm 1$	$49 \pm 1$
Single-photon detection	$38 \pm 1$	$30 \pm 1$
Total	$3.5 \pm 0.3$	$4.0 \pm 0.2$

From the above coincidence-spectrum measurements and knowledge of the channel efficiencies, one can extract the photon-pair component from the single-photon fluorescence component in each channel. We denote  $\eta_s$  ( $\eta_i$ ) as the total efficiency (including all collection and detection losses) for the signal (idler) photon channels. The photon-pair contribution to the total photon flux produced by the waveguide can be written as:  $N_2 = (N_c \cdot F)/(\eta_s \cdot \eta_i)$ , where  $N_c \equiv C - A$  is the detected true coincidence rate and  $F = 80$  is the down-count factor from the laser repetition rate. The single-photon fluorescence production rate can be calculated by subtracting the photon-pair rate from the total production rate in each channel:  $N_{1(s)} = D_s/\eta_s - N_2$  and  $N_{1(i)} = D_i \cdot F/\eta_i - N_2$ , where  $D_s$  and  $D_i$  are the dark-count-subtracted detected photon rate in the signal and idler channel, respectively. This technique is similar to the one used in separating four-wave-mixing photon pairs from spontaneous Raman

scattering in the context of fiber-based  $\chi^{(3)}$  photon-pair sources.<sup>38,39</sup> In the following, we apply this to our waveguide-based  $\chi^{(2)}$  photon-pair source, and for the first time give a complete and separate description of the SPDC photon spectrum and fluorescence spectrum for the entire down-conversion bandwidth, for both types of SPDC.

The results in Fig. 5 show the relative strength of down-converted photon pair and single-photon fluorescence for type-0 SPDC at its optimal temperature [Fig. 5(a)] and type-II SPDC at three different temperatures [Fig. 5(b), (c), (d)]. In the analysis, we used the experimentally determined total collection efficiencies  $\eta_s = 3.5\% \pm 0.3\%$  and  $\eta_i = 4.0\% \pm 0.2\%$ . The details of the measured efficiencies are listed in Table 1. These efficiencies were measured for a pair of wavelengths  $\lambda_s = 900$  nm and  $\lambda_i = 1300$  nm using classical light at those wavelengths. It is possible that these efficiencies are dependent on the wavelength of light that is collected. However, since the majority of the down-converted 1300 nm (900 nm) light is emitted in a single spatial mode, and falls within the 12 nm and 1.4 nm (6 nm and 0.7 nm) 3-dB passbands for type-0 and type-II SPDC, respectively, we assume the collection efficiencies are constant within those passbands. It can be clearly seen that when operating at the optimal temperature, the photon-pair component is much higher than the single-photon fluorescence component. On the other hand, the single-photon fluorescence can become comparable to or even higher than the former when the waveguide is away from the optimal temperature or the photon wavelength falls outside the SPDC phase-matching band.

Table 2: Comparison of spectral brightness efficiencies for both type-0 and type-II SPDC for our waveguide versus the results of others (Refs. [12, 40, 41]). Note that while Ref. [41] specifies an *in-fiber* spectral brightness efficiency, all other numbers are *pair-production* spectral brightness efficiencies (i.e., without coupling into single-mode fibers).

References	SPDC spectral brightness efficiency ( $10^6$ /s/mW/THz)	
	type-0	type-II
Previous work	3 [41]	160 [12, 40]
This work	83	250

From Fig. 5 we can also estimate our source's spectral brightness per mW of pump power exiting the waveguide, which we define as "spectral brightness efficiency." The pair-production spectral brightness efficiency for the optimal temperature and the peak wavelength pair for type-0 SPDC and for type-II SPDC are the highest spectral brightness efficiencies reported to date (shown in Table 2).

### 3.5 Quasi-phase matching for type-0 and type-II SPDC

To further our understanding of the physical mechanisms of QPM in the PPKTP waveguide, we numerically calculate the phase-matching curves for both types of SPDC using the Sellmeier equations for flux-grown bulk PPKTP given in Ref. [42]. As depicted in Fig. 6(a),  $x$  is the light propagation direction in the waveguide,  $y$  is the horizontal polarization, and  $z$  is the vertical polarization. The Sellmeier equations for  $y$ -polarized and  $z$ -polarized light fields in the PPKTP waveguide are:<sup>42</sup>

$$n_y(\lambda) = \sqrt{2.19229 + \frac{0.83547}{1 - 0.04970 \lambda^{-2}} - 0.01621 \lambda^2}, \quad (1)$$

$$n_z(\lambda) = \sqrt{2.25411 + \frac{1.06543}{1 - 0.05486 \lambda^{-2}} - 0.02140 \lambda^2}, \quad (2)$$

where  $n_y(z)$  is the refractive index for  $y$  ( $z$ )-polarized light. The phase-matching equations for type-0 and type-II SPDC in the waveguide are given by:

$$\frac{2\pi n_z(\lambda_p)}{\lambda_p} = \frac{2\pi n_z(\lambda_s)}{\lambda_s} + \frac{2\pi n_z(\lambda_i)}{\lambda_i} + \frac{2\pi m_0}{\Lambda} + k_{wg}, \quad (3)$$

$$\frac{2\pi n_y(\lambda_p)}{\lambda_p} = \frac{2\pi n_z(\lambda_s)}{\lambda_s} + \frac{2\pi n_y(\lambda_i)}{\lambda_i} + \frac{2\pi m_2}{\Lambda} + k_{wg}, \quad (4)$$

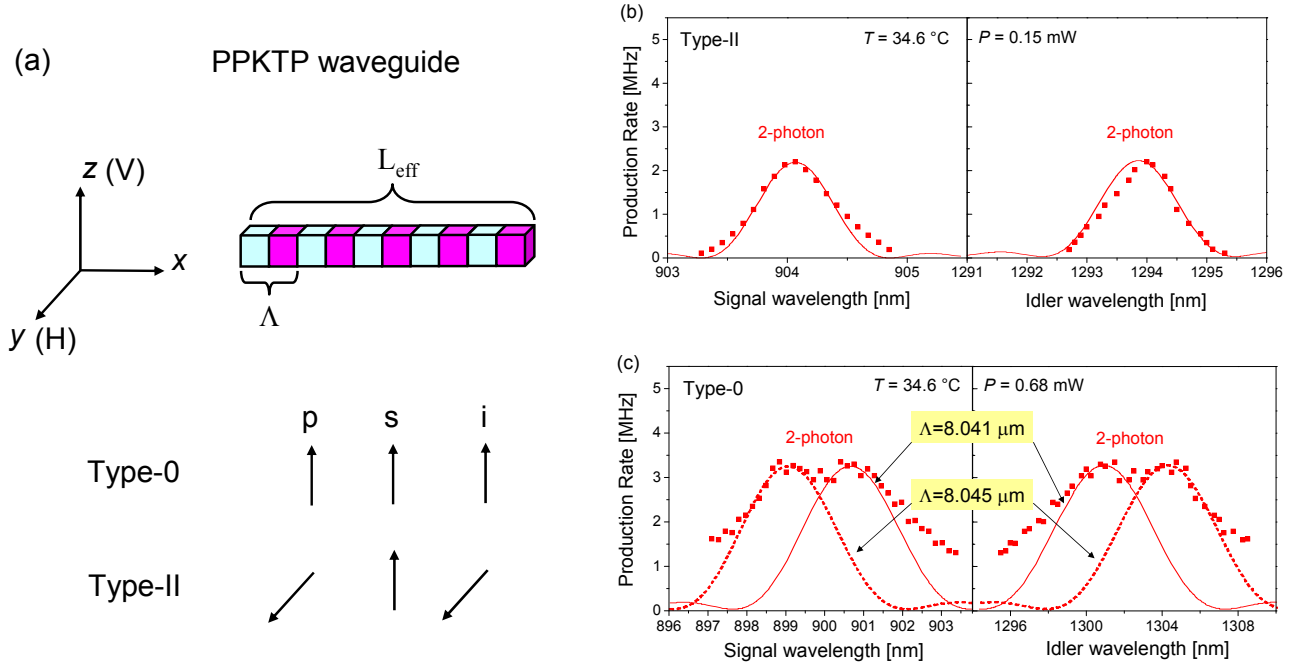


Figure 6: (a) Schematic of the two types of phase matching schemes inside our PPKTP waveguide. Quasi-phase matching functions adjusted to match the photon-pair components obtained from experimental data for (b) type-II SPDC at  $T_{\text{opt}} = 34.6^\circ\text{C}$ , and (c) type-0 SPDC at  $T_{\text{opt}} = 34.6^\circ\text{C}$ . Solid squares are data points for photon-pair components derived from Fig. 5. Fit parameters are  $L_{\text{eff}} = 8.5\text{ mm}$  and  $k_{\text{wg}} = -0.1\ \mu\text{m}^{-1}$  for all curves in (b) and (c). The dashed and the solid curve in (c) use the poling period values indicated.

where the wavelengths are in microns, and  $m_0$  ( $m_2$ ) is the (integer) order of grating harmonic that contributes to phase matching in type-0 (type-II) SPDC.

In the above equations, we assume the waveguide contribution  $k_{\text{wg}}$  to phase matching is the same for the two types of SPDC, which is a valid assumption since the wavelengths involved are very close. Solving Eqs. (3) and (4) simultaneously, we find valid solutions *only when*  $m_0 = 1$  and  $m_2 = 0$ . This means that type-II phase matching does not need any contribution from periodic poling, and therefore picks up the 0th-order harmonic of the grating ( $m_2 = 0$ ), whereas type-0 phase matching is made possible by the contribution from the first-order harmonic of the grating ( $m_0 = 1$ ).

Putting the peak phase matching wavelengths for type-II SPDC ( $\lambda_p = 0.5322\ \mu\text{m}$ ,  $\lambda_s = 0.904\ \mu\text{m}$ , and  $\lambda_i = 1.294\ \mu\text{m}$ ) into Eq. (4) determines the waveguide contribution to be  $k_{\text{wg}} = -0.1\ \mu\text{m}^{-1}$ . Similarly, by plugging the peak phase matching wavelengths for type-0 SPDC ( $\lambda_p = 0.5322\ \mu\text{m}$ ,  $\lambda_s = 0.8992\ \mu\text{m}$ , and  $\lambda_i = 1.304\ \mu\text{m}$ ) into Eq. (3), we determine the fit value of the grating period to be  $\Lambda \approx 8.045\ \mu\text{m}$ . This is less than the nominal value of  $8.29\ \mu\text{m}$  given by the manufacturer, and we attribute this difference to the temperature dependence of the grating period and possible variations in the periodic poling process (since the poling period is only microns long, there may be variations in uniformity of pole widths and periods).

In the CW pump limit (a good approximation for our pump due to its narrow bandwidth), the signal and idler spectra are given by the function  $\text{sinc}^2(\Delta k L_{\text{eff}}/2)$ , where  $\Delta k = k_p - k_s - k_i - k_{\text{wg}}$  for type-II SPDC and  $\Delta k = k_p - k_s - k_i - 2\pi/\Lambda - k_{\text{wg}}$  for type-0 SPDC. We use these to generate phase matching curves for both signal and idler fields to fit the experimental data shown in Fig. 6(b) and (c). The matching between theory and experiment is remarkably good. An effective length of the entire waveguide of  $L_{\text{eff}} = 8.5\text{ mm}$  matches the experimental FWHM of type-II SPDC. This length is significantly shorter than the specified nominal length of  $15\text{ mm}$ , suggesting possible variation in the waveguide fabrication.<sup>20</sup>

The data in Fig. 6(c) is compared to two curves with different grating periods. We can see that a tiny change in the grating period ( $\Delta\Lambda = 4\text{ nm}$ ,  $\Delta\Lambda/\Lambda \approx 0.0005$ ) alters the phase matching wavelengths by a considerable

amount ( $\Delta\lambda_s \approx 2$  nm,  $\Delta\lambda_i \approx 4$  nm). We thus believe that the broadening of type-0 SPDC phase matching bandwidth is due to some small non-uniformity in the grating period over the waveguide.<sup>20</sup> As type-II phase matching does *not* depend on periodic poling, a variation in grating period will not affect the bandwidth of type-II SPDC. This is supported by the data matching a single  $\text{sinc}^2(\Delta k L_{\text{eff}}/2)$  function in Fig. 6(b). Temperature tuning affects the type-II SPDC spectra through the temperature dependence inherent in the refractive indices  $n(\lambda, T)$ ,<sup>20</sup> and by altering the waveguide contribution  $k_{\text{wg}}(T)$ , while the temperature dependence of the grating period  $\Lambda(T)$  does not affect the type-II spectra because type-II SPDC does not depend on the poling period. In comparison, the type-0 SPDC spectra is affected by the temperature tuning through  $n(\lambda, T)$ ,  $k_{\text{wg}}(T)$ , and also  $\Lambda(T)$ . We believe the main reason for type-II SPDC to be brighter (both spectrally and overall) than its type-0 counterpart in this waveguide (despite  $d_{\text{eff}} > d_{24}$ ) is that the difficulty in maintaining a uniform grating period and the resulting variations in the grating period along the entire waveguide effectively decreases the phase matching efficiency of type-0 SPDC, with different sections of the waveguide producing photon pairs at different wavelengths which do not add up coherently. Since type-II SPDC is immune to the grating period change, it is enhanced relative to its type-0 counterpart.

#### 4. PRELIMINARY RESULTS FOR 1.55 $\mu\text{M}$ -0.8 $\mu\text{M}$ PHOTON PAIRS

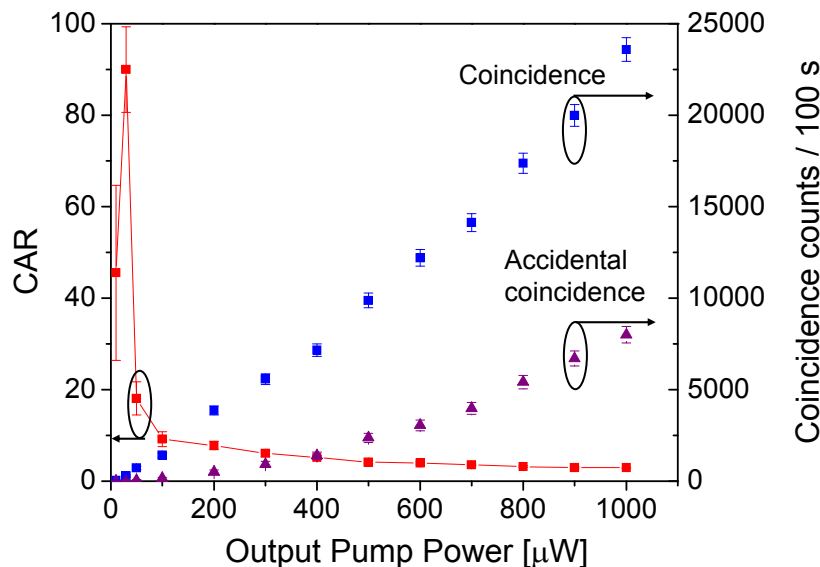


Figure 7: Pump power dependencies of CAR (left axis) and coincidences and accidental coincidences per 100 s (right axis) for type-0 SPDC with  $\lambda_s = 808.7$  nm and  $\lambda_i = 1557.4$  nm. The red line is a guide to the eye. Detector dark-count contributions have been subtracted.

Here we describe our preliminary results in generating photon pairs with  $\lambda_s \sim 810$  nm and  $\lambda_i \sim 1550$  nm. We used a different PPKTP waveguide (7 mm long,  $4 \times 4 \mu\text{m}^2$  cross section) specifically designed to quasi-phase-match type-0 SPDC for the above wavelengths with  $\lambda_p \sim 532$  nm. Having one of the down-converted photons reside in the 1550-nm telecom band takes full advantage of the lowest propagation loss window in fused-silica optical fiber, making the source useful for long-distance quantum communication applications.

The experimental setup is very similar to the one shown in Fig. 1, except the tunable bandpass filters are now configured to be compatible with the wavelengths of interest. The home-made signal filter bandwidth is set to  $\Delta\lambda_s = 0.8$  nm to match the fixed commercial idler filter bandwidth  $\Delta\lambda_i = 2$  nm. The waveguide is, however, *not* temperature stabilized, since at the time of the experiment the thermo-electric cooler was not available. Due to the absence of temperature control, the obtained photon counts are less than optimal, since the waveguide just sits at room temperature ( $\approx 25^\circ\text{C}$ ) and its phase matching can be easily affected by ambient temperature fluctuations.

Figure 7 depicts a typical experimental result for this waveguide without temperature control. The coincidence and accidental coincidence counts were taken at the peak wavelength pair  $\{\lambda_s = 808.7 \text{ nm}, \lambda_i = 1557.4 \text{ nm}\}$ . Their ratio, CAR, is calculated and shown on the same figure. The CAR peaks at  $\approx 90$  at an average pump power of  $30 \mu\text{W}$ . Below this pump power the CAR starts to decrease, which we believe is due to the low photon counts approaching the detection sensitivity limit. Comparing this result with those in Fig. 3, we see that this result is inferior in terms of spectral brightness as well as CAR. There are at least three possible reasons for this: (i) this waveguide has intrinsically lower  $\chi^{(2)}$  nonlinearity for producing photon pairs, (ii) ambient temperature fluctuations affect the output photon pair production, and (iii) we have not tuned the waveguide to its optimal phase-matching temperature. We believe it is likely to be a combination of all of them. Assuming that the two waveguides have similar  $\chi^{(2)}$  nonlinearity, the sharp contrast between the two sets of results proves the importance of having stable, tunable temperature control for the waveguide.

## 5. CONCLUSION

We have demonstrated a potentially useful device for chip-scale quantum information processing by measuring a single PPKTP waveguide's output spectra (single and coincidence) at a range of operating temperatures, pump powers, and phase-matching schemes. The results show a versatile device, which has a tunable central wavelength and a choice between a narrow or broad bandwidth, together with high spectral brightness and high purity. We have separated the photon-pair contribution from single-photon fluorescence for both type-0 and type-II SPDC. This single-photon fluorescence may result from defects in the PPKTP crystal such as gray tracking and/or color center formation,<sup>6,43</sup> although a definitive answer is not possible at the moment. We have also investigated a waveguide without temperature stabilization, whose inferior results prove the necessity of having temperature control for waveguided SPDC.

Future research will investigate a waveguide made from a hydrothermally-grown KTP crystal, because it may produce fewer single-photon fluorescence than the flux-grown one that we used. This can potentially yield a photon-pair source with even higher purity. Improving collection efficiencies (including both free-space and fiber-coupling optics) will boost the collected photon-pair rate, and thus the usable brightness of the source. It might be possible to spectrally engineer the type-II SPDC output from the waveguide to yield a factorable state. We believe such a versatile photon-pair source is a promising candidate for future integrated photonic circuitry and chip-scale quantum devices.

## Acknowledgement

We thank Dr. Tracy Clement for supplying the Matlab codes for calculating the Schmidt numbers and the values for entropy of entanglement, and Dr. Sergey Polyakov and Dr. Wei Fang for helpful discussions. This work has been supported in part by the Intelligence Advanced Research Projects Activity (IARPA) Polarization-Entangled Photon Source Program, and the Multidisciplinary University Research Initiative Center for Photonic Quantum Information Systems (Army Research Office/IARPA program DAAD19-03-1-0199). A.J.P. acknowledges support from the Intelligence Community Postdoctoral Research Associateship Program.

## REFERENCES

- [1] P. G. Kwiat, K. Mattle, H. Weinfurter, A. Zeilinger, A. V. Sergienko, and Y. Shih, "New High-Intensity Source of Polarization-Entangled Photon Pairs," *Phys. Rev. Lett.* **75**, 4337-4341 (1995).
- [2] T. E. Kiess, Y. H. Shih, A. V. Sergienko, and C. O. Alley, "Einstein-Podolsky-Rosen-Bohm Experiment Using Pairs of Light Quanta Produced by Type-II Parametric Down-conversion," *Phys. Rev. Lett.* **71**, 3893-3897 (1993).
- [3] H. Takesue and K. Inoue, "Generation of polarization-entangled photon pairs and violation of Bell's inequality using spontaneous four-wave mixing in a fiber loop," *Phys. Rev. A* **70**, 031802(R) (2004).
- [4] X. Li, P. L. Voss, J. E. Sharping, and P. Kumar, "Optical-Fiber Source of Polarization-Entangled Photons in the 1550 nm Telecom Band," *Phys. Rev. Lett.* **94**, 053601 (2005).
- [5] A. L. Migdall, D. Branning, and S. Castelletto, "Tailoring single-photon and multiphoton probabilities of a single-photon on-demand source," *Phys. Rev. A* **66**, 053805 (2002).

- [6] A. B. U'Ren, C. Silberhorn, K. Banaszek, and I. A. Walmsley, "Efficient Conditional Preparation of High-Fidelity Single Photon States for Fiber-Optic Quantum Networks," *Phys. Rev. Lett.* **93**, 093601 (2004).
- [7] E. Knill, R. LaFlamme, and G. J. Milburn, "A scheme for efficient quantum computation with linear optics," *Nature* **409**, 46-52 (2001).
- [8] P. Kok, W. J. Munro, K. Nemoto, T. C. Ralph, and G. J. Milburn, "Linear optical quantum computing with photonic qubits," *Rev. Mod. Phys.* **79**, 135-174 (2007).
- [9] K. Banaszek, A. B. U'Ren, and I. A. Walmsley, "Generation of correlated photons in controlled spatial modes by downconversion in nonlinear waveguides," *Opt. Lett.* **26**, 1367-1369 (2001).
- [10] S. Tanzilli, H. De Riedmatten, W. Tittel, H. Zbinden, P. Baldi, M. De Micheli, D.B. Ostrowsky, and N. Gisin, "Highly efficient photon-pair source using periodically poled lithium niobate waveguide," *Electron. Lett.* **37**, 26-28 (2001).
- [11] K. Sanaka, K. Kawahara, and T. Kuga, "New High-Efficiency Source of Photon Pairs for Engineering Quantum Entanglement," *Phys. Rev. Lett.* **86**, 5620-5623 (2001).
- [12] M. Fiorentino, S. M. Spillane, R. G. Beausoleil, T. D. Roberts, P. Battle, and M. W. Munro, "Spontaneous parametric down-conversion in periodically poled KTP waveguides and bulk crystals," *Opt. Express* **15**, 7479-7488 (2007).
- [13] Q. Zhang, X. Xie, H. Takesue, S. W. Nam, C. Langrock, M. M. Fejer, and Y. Yamamoto, "Correlated photon-pair generation in reverse-proton-exchange PPLN waveguides with integrated mode demultiplexer at 10 GHz clock," *Opt. Express* **15**, 10288-10293 (2007).
- [14] C. Liang, K. F. Lee, J. Chen, and P. Kumar, "Distribution of Fiber-Generated Polarization Entangled Photon-Pairs over 100 km of Standard Fiber in OC-192 WDM Environment," postdeadline paper presented at OFC 2006, paper PDP35.
- [15] S. Sauge, M. Swillo, S. Albert-Seifried, G. B. Xavier, J. Waldebäck, M. Tengner, D. Ljunggren, and A. Karlsson, "Narrowband polarization-entangled photon pairs distributed over a WDM link for qubit networks," *Opt. Express* **15**, 6926-6933 (2007).
- [16] W. P. Grice and I. A. Walmsley, "Spectral information and distinguishability in type-II down-conversion with a broadband pump," *Phys. Rev. A* **56**, 1627-1634 (1997).
- [17] Y. Kim and W. P. Grice, "Measurement of the spectral properties of the two-photon state generated via type II spontaneous parametric downconversion," *Opt. Lett.* **30**, 908-910 (2005).
- [18] H. S. Poh, C. Y. Lum, I. Marcikic, A. Lamas-Linares, and C. Kurtsiefer, "Joint spectrum mapping of polarization entanglement in spontaneous parametric down-conversion," *Phys. Rev. A* **75**, 043816 (2007).
- [19] A. Ling, P. Y. Han, A. Lamas-Linares, and C. Kurtsiefer, "Preparation of Bell States with controlled white noise," *Laser Phys.* **16**, 1140-1144 (2006).
- [20] M. M. Fejer, G. A. Magel, D. H. Jundt, and R. L. Byer, "Quasi-phase-matched second harmonic generation: tuning and tolerances," *IEEE J. Quantum Electron.* **28**, 2631-2654 (1992).
- [21] J. D. Bierlein and H. Vanherzeele, "Potassium titanyl phosphate: properties and new applications," *J. Opt. Soc. Am. B* **6**, 622-633 (1989).
- [22] M. Ghioni, A. Gulinatti, I. Rech, F. Zappa, and S. Cova, "Progress in silicon single-photon avalanche diodes," *IEEE J. Sel. Top. Quantum Electron.* **13**, 852-862 (2007).
- [23] K. M. Rosfjord, J. K. W. Yang, E. A. Dauler, A. J. Kerman, V. Anant, B. M. Voronov, G. N. Gol'tsman, and K. K. Berggren, "Nanowire single-photon detector with an integrated optical cavity and anti-reflection coating," *Opt. Express* **14**, 527-534 (2006).
- [24] A. E. Lita, A. J. Miller, and S. W. Nam, "Counting near-infrared single-photons with 95% efficiency," *Opt. Express* **16**, 3032-3040 (2008).
- [25] A. Christ, K. Laiho, A. Eckstein, T. Lauckner, P. J. Mosley, and C. Silberhorn, "Spatial modes in waveguided parametric downconversion", arXiv:0904.4668v1.
- [26] J. Chen, K. F. Lee, C. Liang, and P. Kumar, "Fiber-based telecom-band degenerate-frequency source of entangled photon pairs," *Opt. Lett.* **31**, 2798-2800 (2006).
- [27] J. Fan, A. Dogariu, and L. J. Wang, "Generation of correlated photon pairs in a microstructure fiber," *Opt. Lett.* **30**, 1530-1532 (2005).

- [28] K. F. Lee, J. Chen, C. Liang, X. Li, P. L. Voss, and P. Kumar, "Generation of high-purity telecom-band entangled photon pairs in dispersion-shifted fiber," *Opt. Lett.* **31**, 1905-1907 (2006).
- [29] H. Takesue and K. Inoue, "1.5- $\mu\text{m}$  band quantum-correlated photon pair generation in dispersion-shifted fiber: suppression of noise photons by cooling fiber," *Opt. Express* **13**, 7832-7839 (2005).
- [30] S. D. Dyer, M. J. Stevens, B. Baek, and S. W. Nam, "High-efficiency, ultra low-noise all-fiber photon-pair source," *Opt. Express* **16**, 9966-9977 (2008).
- [31] J. Chen, X. Li, and P. Kumar, "Two-photon-state generation via four-wave mixing in optical fibers," *Phys. Rev. A* **72**, 033801 (2005).
- [32] D. C. Burnham and D. L. Weinberg, "Observation of Simultaneity in Parametric Production of Optical Photon Pairs," *Phys. Rev. Lett.* **25**, 84-87 (1970).
- [33] We note that another method for measuring joint spectrum is given by W. Wasilewski *et. al.*, "Joint spectrum of photon pairs measured by coincidence Fourier spectroscopy," *Opt. Lett.* **31**, 1130-1132 (2006).
- [34] C. K. Law, I. A. Walmsley, and J. H. Eberly, "Continuous frequency entanglement: effective finite Hilbert space and entropy control," *Phys. Rev. Lett.* **84**, 5304-5307 (2000).
- [35] A. B. U'Ren, C. Silberhorn, K. Banaszek, I. A. Walmsley, R. Erdmann, W. P. Grice, and M. G. Raymer, "Generation of pure-state single-photon wavepackets by conditional preparation based on spontaneous parametric downconversion," *Laser Phys.* **15**, 146-161 (2005).
- [36] A. Ekert and P. L. Knight, "Entangled quantum systems and the Schmidt decomposition," *Am. J. Phys.* **63**, 415-423 (1995).
- [37] A. B. U'Ren, K. Banaszek, and I. A. Walmsley, "Photon engineering for quantum information processing," *Quant. Inf. and Comp.* **3**, 480-502 (2003).
- [38] X. Li, P. L. Voss, J. Chen, K. F. Lee, and P. Kumar, "Measurement of co- and cross-polarized Raman spectra in silica fiber for small detunings," *Opt. Express* **13**, 2236-2244 (2005).
- [39] J. Fan and A. Migdall, "A broadband high spectral brightness fiber-based two-photon source," *Opt. Express* **15**, 2915-2920 (2007).
- [40] A. Fedrizzi, T. Herbst, A. Poppe, T. Jennewein, and A. Zeilinger, "A wavelength-tunable fiber-coupled source of narrowband entangled photons," *Opt. Express* **15**, 15377-15386 (2007).
- [41] S. Sauge, M. Swillo, M. Tengner, and A. Karlsson, "A single-crystal source of path-polarization entangled photons at non-degenerate wavelengths," *Opt. Express* **16**, 9701-9707 (2008).
- [42] T. Y. Fan, C. E. Huang, B. Q. Hu, R. C. Eckardt, Y. X. Fan, R. L. Byer, and R. S. Feigelson, "Second harmonic generation and accurate index of refraction measurements in flux-grown  $\text{KTiOPO}_4$ ," *App. Opt.* **26**, 2390-2394 (1987).
- [43] B. Boulanger, I. Rousseau, J. P. Fève, M. Maglione, B. Menaert, G. Marnier, "Optical Studies of Laser-Induced Gray-Tracking in KTP," *IEEE J. Quantum Electron.* **35**, 281-286 (1999).